Cell

ATR Prohibits Replication Catastrophe by Preventing Global Exhaustion of RPA

Luis Ignacio Toledo,[1] Matthias Altmeyer,[1] Maj-Britt Rask,[1] Claudia Lukas,[1] Dorthe Helena Larsen,[1] Lou Klitgaard Povlsen,[2] Simon Bekker-Jensen,[2] Niels Mailand,[2] Jiri Bartek,[3,4] and Jiri Lukas[1,*]
[1]Chromosome Stability and Dynamics Group
[2]Ubiquitin Signaling Group
Novo Nordisk Foundation Center for Protein Research, Faculty of Health and Medical Sciences, University of Copenhagen, Blegdamsvej 3B, 2200 Copenhagen, Denmark
[3]Genome Integrity Unit, Danish Cancer Society Research Center, Strandboulevarden 49, 2100, Copenhagen, Denmark
[4]Institute of Molecular and Translational Medicine, Faculty of Medicine, Palacky University, 775 15 Olomouc, Czech Republic
*Correspondence: jiri.lukas@cpr.ku.dk
http://dx.doi.org/10.1016/j.cell.2013.10.043

SUMMARY

ATR, activated by replication stress, protects replication forks locally and suppresses origin firing globally. Here, we show that these functions of ATR are mechanistically coupled. Although initially stable, stalled forks in ATR-deficient cells undergo nucleus-wide breakage after unscheduled origin firing generates an excess of single-stranded DNA that exhausts the nuclear pool of RPA. Partial reduction of RPA accelerated fork breakage, and forced elevation of RPA was sufficient to delay such "replication catastrophe" even in the absence of ATR activity. Conversely, unscheduled origin firing induced breakage of stalled forks even in cells with active ATR. Thus, ATR-mediated suppression of dormant origins shields active forks against irreversible breakage via preventing exhaustion of nuclear RPA. This study elucidates how replicating genomes avoid destabilizing DNA damage. Because cancer cells commonly feature intrinsically high replication stress, this study also provides a molecular rationale for their hypersensitivity to ATR inhibitors.

INTRODUCTION

Eukaryotic genomes are constantly challenged by assaults that can undermine the integrity of replicating DNA. Mild forms of replication stress stochastically occur during physiological cell cycles, and pathological settings such as oncogenic transformation further elevate replication stress, which could lead to DNA damage and instigate genomic instability (Halazonetis et al., 2008). The common denominator of replication stress is a stalled fork, an aberrant structure that triggers a genome surveillance pathway orchestrated by the ATR kinase (Branzei and Foiani, 2009). ATR is activated by its physical recruitment to RPA-coated single-stranded DNA (ssDNA) generated by uncoupling of replicative MCM helicase from DNA polymerases. ATR and its downstream effectors are then required to counteract adverse effects of replication stress both by delaying cell-cycle progression and by stabilizing stalled forks (Friedel et al., 2009). Consequences of impaired ATR signaling include chromosome instability, developmental defects, and accelerated aging (Brown and Baltimore, 2000; Murga et al., 2009). Furthermore, ATR signaling has been implicated in oncogenesis by imposing a barrier to cancer progression (Fang et al., 2004). However, although the ATR pathway is clearly central for genome maintenance, how it protects replicating DNA is not well understood.

ATR signaling must be carefully choreographed on a temporal scale. Replication stress is a highly dynamic chain of events starting from acutely arrested forks with fully assembled replisomes. If replication stress persists, stalled forks are converted into "collapsed forks" characterized by dissociation and/or impaired modifications of replisome components (Lambert and Carr, 2005; Tercero et al., 2003). Further extension of replication stress can convert forks to DNA double-strand breaks (DSBs) that pose the most serious threat to genome integrity. It has been shown that the latter transition requires cleavage of replication intermediates by structure-specific nucleases such as SLX4 and MUS81 (Fekairi et al., 2009; Forment et al., 2011; Hanada et al., 2007) and that ATR signaling delays the onset of fork breakage (Trenz et al., 2006). However, it is also evident from these studies that replication fork breakage is a delayed response that develops only over many hours (Petermann et al., 2010). Why the fork protection initially works and eventually fails is currently unknown.

The spatial aspect of ATR signaling brings about another layer of complexity. The ATR pathway not only regulates fork stability locally, but one of its signaling components, the CHK1 kinase, diffuses globally through the nucleus, where it counteracts new origin firing (Sørensen and Syljuåsen, 2012). The unresolved question is how are the "local" (short range, at stalled forks) and "global" (long range, throughout the nucleus) functions of

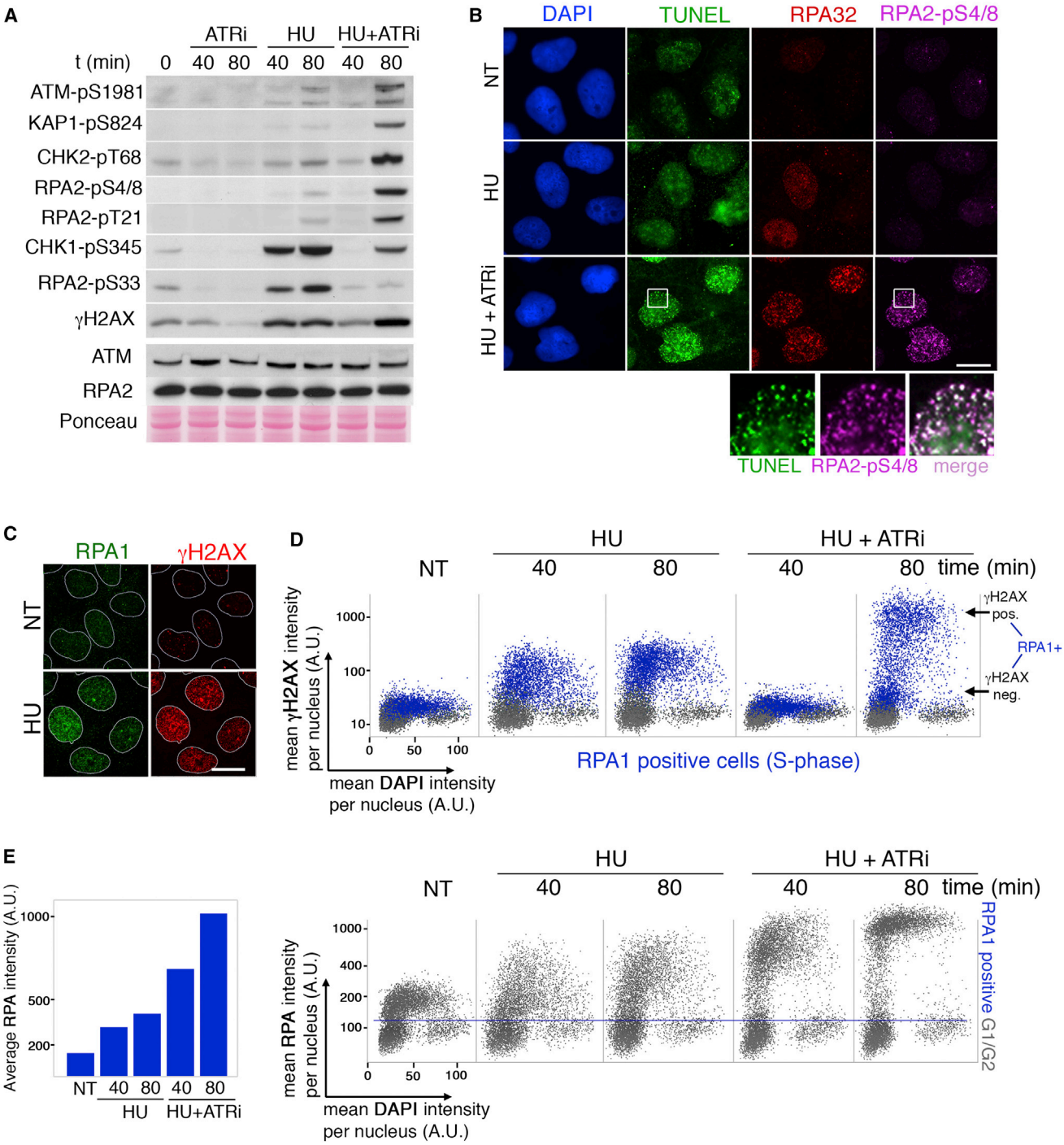

Figure 1. ATR Inhibition Triggers Hyperloading of RPA on S Phase Chromatin followed by Fork Breakage

(A) Asynchronous U-2-OS cells were incubated with HU (2mM) and ATRi (2 μM) for the indicated times. Whole-cell extracts (WCE) were immunoblotted with the indicated antibodies.

(B) U-2-OS cells were incubated with HU ± ATRi for 80 min and immunostained with the indicated antibodies after pre-extraction. DSBs were labeled with a TUNEL assay. Nuclear DNA was counterstained by DAPI. Insets show colocalization of DSBs and RPA2-pS4/8 foci. Scale bar, 10 μm.

(C) U-2-OS cells were treated with HU for 40 min, pre-extracted, and immunostained with the indicated antibodies. Scale bar, 10 μm.

(D) Quantitative *i*mage-*b*ased *c*ytometry single-cell *a*nalysis (QIBC) of immunolabeled U-2-O-S cells. Asynchronous cells were treated with HU (2 mM) and ATRi (2 μM) for the indicated times and immunostained as in (C). Mean nuclear intensities for DAPI, RPA1 (chromatin-bound fraction [CB]), and γ-H2AX were determined for each of >5,000 individual cells and were plotted in a scatter diagram. S phase cells, with chromatin-loaded RPA1, are labeled in blue.

(legend continued on next page)

ATR coordinated. In this study, we provide evidence that the global and local functions of ATR converge at a surprisingly simple but robust mechanism, which effectively guards the genome against destabilizing replication stress.

RESULTS

Stalled Forks Are Transiently Resistant to Breakage Independent of ATR Signaling

To investigate mechanisms involved in replication fork stability, we induced replication stress by treating U-2-OS cells with hydroxyurea (HU), which causes rapid depletion of dNTPs (Eklund et al., 2001). To manipulate ATR activity, we applied a specific ATR inhibitor (ATRi), which faithfully recapitulates phenotypes associated with genetic ablation of ATR (Toledo et al., 2011). In addition to inducing gradual phosphorylation of ATR targets such as H2AX (pS139), CHK1 (pS345), and RPA2 (pS33) (Figure 1A), combination of HU with ATRi resulted in a delayed phosphorylation of ATM targets, including ATM (pS1981), KAP1 (pS824), CHK2 (pT68), and RPA2 (pT21, pS4/8). This was accompanied by generation of DSBs detected by the TUNEL assay specifically at the RPA-decorated stalled forks with hallmarks of ATM activity (Figure 1B). Whereas fork breakage in ATR-deficient cells was expected, it was surprising to see that this occurred with a substantial delay (Figure 1) despite the kinase being inhibited within seconds to minutes (Toledo et al., 2011). This raised the possibility that, for a limited period of time, the fork protection machinery operates autonomously and independently of ATR.

To investigate this possibility, we established a quantitative image-based cytometry (QIBC) method, which allowed us to monitor the complete dynamics of replication stress responses with unprecedented detail and in a fully automated and high content-fashion (see Supplemental Information available online). The key feature of this assay is its ability to separate with great accuracy and reproducibility the fraction of cells with intact stalled forks from those in which the combination of HU and ATRi treatment triggered fork breakage accompanied by hallmarks of ATM activity such as H2AX hyperphosphorylation (Figures 1C and 1D). Interestingly, also at this analytical level, the conversion of stalled forks to DSBs lagged behind acute ATR inhibition (Figures S1A and S1B), and we therefore set out to investigate the mechanistic underpinnings of fork surveillance between ATR inhibition and DSB generation.

Breakage of Stalled Forks Correlates with Increased Levels of Chromatin-Loaded RPA

We noticed that, before DSBs became detectable, the amount of RPA loaded on chromatin accumulated to levels that were several fold higher than in cells exposed to HU alone (Figure 1E). Increasing the HU concentration did not further increase RPA loading, confirming that replication was fully stalled (Figure S2A). These data allowed for two predictions: (1) that ATR may have a specific role in limiting RPA chromatin loading and (2) that the excessive RPA loading in the absence of ATR might be coupled to DSB generation. Consistent with these predictions, the accumulation of RPA on chromatin reached its peak well before DSB generation, and the conversion of stalled forks to DSBs was confined to cells with the highest degree of chromatin-loaded RPA both in U-2-OS cells, used as a model system throughout this study (Figures 2A, 2B, and S2B), and in primary, nonimmortalized human fibroblasts (Figure 2C). Furthermore, we reproduced these results by knocking down ATR with siRNA (Figures S2C and S2D) and in DLD1-ATR-*Seckel* cells carrying a hypomorphic *Atr* mutation (Hurley et al., 2007) (Figure S2E). Because prolonged dNTP deprivation was reported to trigger DSBs even in cells with intact ATR (Petermann et al., 2010), we applied QIBC on cells treated with HU alone for up to 24 hr. Indeed, we saw progressive accumulation of cells with broken forks in the later time points (Figure 2D), and DSB generation was again restricted to cells with the highest levels of chromatin-loaded RPA (Figures S2F and S2G). Thus, the excessive accumulation of RPA at stalled forks precedes DNA breakage, and ATR delays this pathological outcome of replication stress.

Nuclear Pool of RPA Is Rate Limiting for ssDNA Protection at Stalled Forks

Because RPA avidly interacts with ssDNA (Fanning et al., 2006), we considered the possibility that ATR inhibition might increase ssDNA generation up to the point where it would deplete all available RPA. Initially, generation of ssDNA detected by BrdU incorporation under nondenaturing conditions (Figure 2E) and accumulation of chromatin-loaded RPA followed an expected linear trend. However, when RPA loading reached its limit, ssDNA continued to accumulate (Figure 2F). This was reflected by a deviation from linearity of the ssDNA/RPA ratio, suggesting that cells reached a stage when RPA became limited for binding newly generated ssDNA. Performing the same assay in a cell line stably expressing RPA2-EGFP allowed us to include a DSB marker (ATM-phosphorylated RPA2-pT21) and thus directly correlate ssDNA formation, RPA loading, and DNA breakage. Remarkably, DSBs were strictly confined to cells that had sequestered all RPA and generated an excess of uncoated ssDNA (Figure 2G). Thus, in the absence of ATR, ssDNA at stalled forks progressively depletes the nuclear pool of RPA, which is accompanied by a conversion of stalled forks to DSBs.

Excessive Origin Firing Depletes RPA and Triggers Simultaneous Fork Breakage in Active Replication Factories

ATR activity is propagated by the CHK1 kinase, which diffuses from stalled forks to restrain origin firing. Although this global spreading of the ATR pathway seems to have limited bearings on local protection of stalled forks, our data indicated a mechanistic connection. First, the increase in chromatin-bound RPA after ATR inhibition could be explained by hyperaccumulation

(E) (Right) Mean RPA1 and DAPI values from (D) are plotted in a scatter diagram. The blue line indicates the threshold used to discriminate S phase from G1 and G2 cells based on chromatin-loaded RPA1 levels. (Left) Average intensities of chromatin-loaded RPA in S phase cells from the scatter diagram.
See also Figure S1.

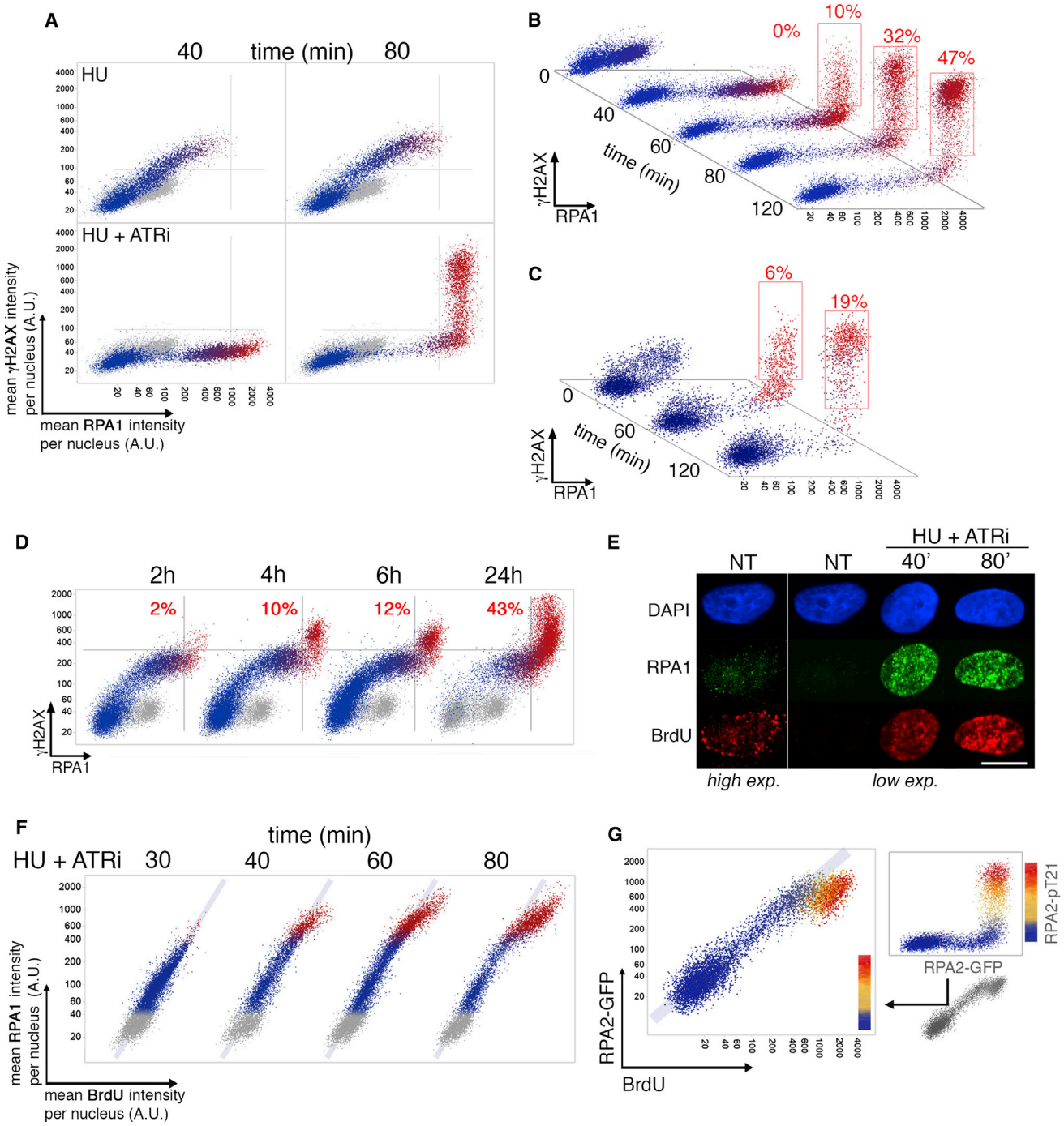

Figure 2. Fork Breakage Occurs when ssDNA Exhausts Nuclear RPA

(A) QIBC of U-2-OS cells. Mean γ-H2AX and RPA fluorescence intensities from Figures 1D and 1E are plotted in a scatter diagram. Coloring indicates RPA levels at which the pool is exhausted, and DSB appear red. Untreated cells are depicted in gray.

(B) QIBC of U-2-OS cells treated for the indicated times with HU (2 mM) and ATRi (2 μM) and immunostained for γ-H2AX and RPA1 after pre-extraction. Mean values are plotted in a scatter diagram. Percentages of ATM-dependent γ-H2AX-positive cells (containing DSBs) were calculated.

(C) QIBC of the BJ primary fibroblasts exposed to HU and ATRi as indicated, and immunostained for γ-H2AX and RPA1 after pre-extraction. Percentages of cells with DSBs were calculated as in (B).

(D) QIBC of U-2-OS cells treated with HU (2 mM) for the indicated times (without ATRi). Percentages of cells with DSBs were calculated as in (B).

(E) U-2-OS cells were grown with BrdU (10 μM) for 48 hr, incubated with HU (2 mM) and ATRi (2 μM) for the indicated times, pre-extracted, and subjected to native BrdU and RPA1 immunostaining to detect ssDNA exposed at replication forks. Scale bar, 10 μm.

(legend continued on next page)

of stalled forks following unscheduled firing of dormant origins (Ge et al., 2007; Ibarra et al., 2008). Second, the rate-limiting nature of RPA would only manifest after excessive origin activity had time to deplete all available RPA, explaining the temporal gap between ATR inhibition and DSB appearance.

To test these predictions, we exploited the paradigm that origin firing requires CDK2 (Gillespie and Blow, 2010). Consistently, application of roscovitine, a broad CDK inhibitor widely used to suppress origin activity, abolished both excessive RPA loading and fork breakage in cells treated with HU and ATRi (Figures 3A, 3B, and S3A). These results were reproduced by inhibiting other regulators of origin firing such as CDC7 or CDC45 (Figures 3A, 3B, S3A, and S3B).The relatively high concentration of HU in all these experiments allowed only minimal fork progression, indicating that the observed effects of roscovitine, CDC7 inhibition, or CDC45 depletion are related to new origin firing. Importantly, substitution of roscovitine by a specific inhibitor of mitotic CDK1 did not prevent fork breakage in HU and ATRi-treated cells (Figure 3C), ruling out the possibility of premature mobilization of structure specific nucleases, which are known to be hyperactivated in mitosis (Matos et al., 2013).

The above results prompted us to ask why some cells tend to exhaust RPA earlier than others. Given the tight correlation between the number of active origins and sequestration of RPA to stalled forks, we hypothesized that cells with the highest replication activity would be the first ones to reach the RPA threshold. Indeed, monitoring of H2AX phosphorylation during the cell cycle revealed that fork breakage after HU and ATRi treatment occurred first in cells with the highest replication rate (Figure 3D). Together, these data suggest that, in the absence of ATR, the coordinated fork breakage occurs during S phase after ssDNA generated by unscheduled origin firing exceeds the nuclear pool of RPA.

Increased Origin Activity Triggers Fork Breakage in ATR-Proficient Cells

In the above experiments, fork breakage was assayed under conditions when HU was combined with ATR inhibition, leaving the possibility that an unknown ATR effector might exert its protective function directly at stalled forks. To address this, we asked whether ATR could have prevented breakage of stalled forks in cells primed to increase the number of active forks above the physiological threshold. We forced otherwise unstressed cells to fire extra origins by transiently inhibiting ATR but without any additional replication stress. Indeed, DNA fiber analysis showed that the number of active forks increased after incubation with ATRi (Figure S3C), and the unscheduled replication was also visible by QIBC as higher levels of chromatin-loaded RPA. Importantly, the time and dose of the ATRi under these conditions did not cause DNA breakage (Figure 3E, time 0). We then washed away the ATRi and incubated, or not, cells with HU. Strikingly, whereas in the absence of replication stress, cells continued to replicate normally, addition of HU rapidly exhausted the residual RPA pool and caused DNA breakage (Figures 3E and S3D). ATR activity recovered back to normal after washing out the inhibitor (Figures 3E and S3E), and roscovitine no longer prevented DSB generation because the majority of available origins had already fired during the priming step (Figure 3F). Thus, the unscheduled origin firing in ATR-deficient cells appears to be the major source of RPA depletion and the ensuing fork breakage.

Exhaustions of RPA Triggers Fork Breakage in All Active Replication Factories

Replication of eukaryotic genomes takes place in replication factories manifesting as nuclear foci that contain both active replicons and dormant origins (Gillespie and Blow, 2010). Given this spatial organization and the emerging evidence that RPA is rate limiting for protecting stalled forks anywhere in the nucleus, our current model predicted that, after all RPA becomes sequestered, unprotected ssDNA should break in all active replication factories. Indeed, this was what we observed. First, in a time-lapse analysis of RPA2-EGFP cells treated with HU and ATRi, we found that RPA progressively accumulated in the same nuclear foci, indicating that the unscheduled origin firing is largely confined to replication factories that were active already at the beginning of the replication stress (Figure 3G and Movies S1, S2, and S3). This was confirmed by comparing the spatial distribution of replication activity before and at the end of replication stress using endogenous RPA (Figure 3H). Second, the hallmarks of fork breakage, such as RPA phosphorylation on S4/8 or T21, occurred simultaneously in all replication factories and regardless of the total extent of damage (Figures 3I, S3F, and S3G). Thus, breakage of stalled forks in a given nucleus after global RPA exhaustion occurs in all replication factories active at the time of replication stress.

Partial Knockdown of RPA Accelerates Breakage of Stalled Forks

To validate these conclusions, we reasoned that lowering RPA levels should render cells more sensitive to excessive origin firing. We partially knocked down RPA1 (Figure 4A) to the degree that did not impair DNA replication, preserved normal ATR activity, and did not cause DNA damage (Figures 4A, S4A, and S4B). Strikingly, however, after applying replication stress by combined HU and ATRi treatment, reduction of RPA levels progressively increased the fraction of cells with DSBs (Figures 4B–4E). We verified that the dynamics of DSB generation closely correlated with accumulation of unprotected ssDNA, consistent with the notion that DNA damage is triggered after ssDNA exceeds

(F) QIBC of U-2-OS images treated and processed as in (E). Mean BrdU and chromatin-loaded RPA1 single-cell values are plotted in a scatter diagram. Progressive deviation of BrdU/RPA1 signal from linearity (light blue bar) is evident in later time points when RPA becomes limiting (red) and leads to exposure of uncoated ssDNA.

(G) QIBC of RPA2-EGFP cells were grown with BrdU as in (E), incubated with HU (2 mM) and ATRi (2 μM) for 100 min, pre-extracted, and immunostained for native BrdU and RPA2-pT21. Mean DAPI, RPA2-EGFP, BrdU, and RPA2-pT21 single-cell values are plotted in the indicated combinations. The RPA2-pT21 color code indicates that the presence of DSBs is confined to cells that deviate from linear RPA2-EGFP/BrdU range (blue bar).

See also Figure S2.

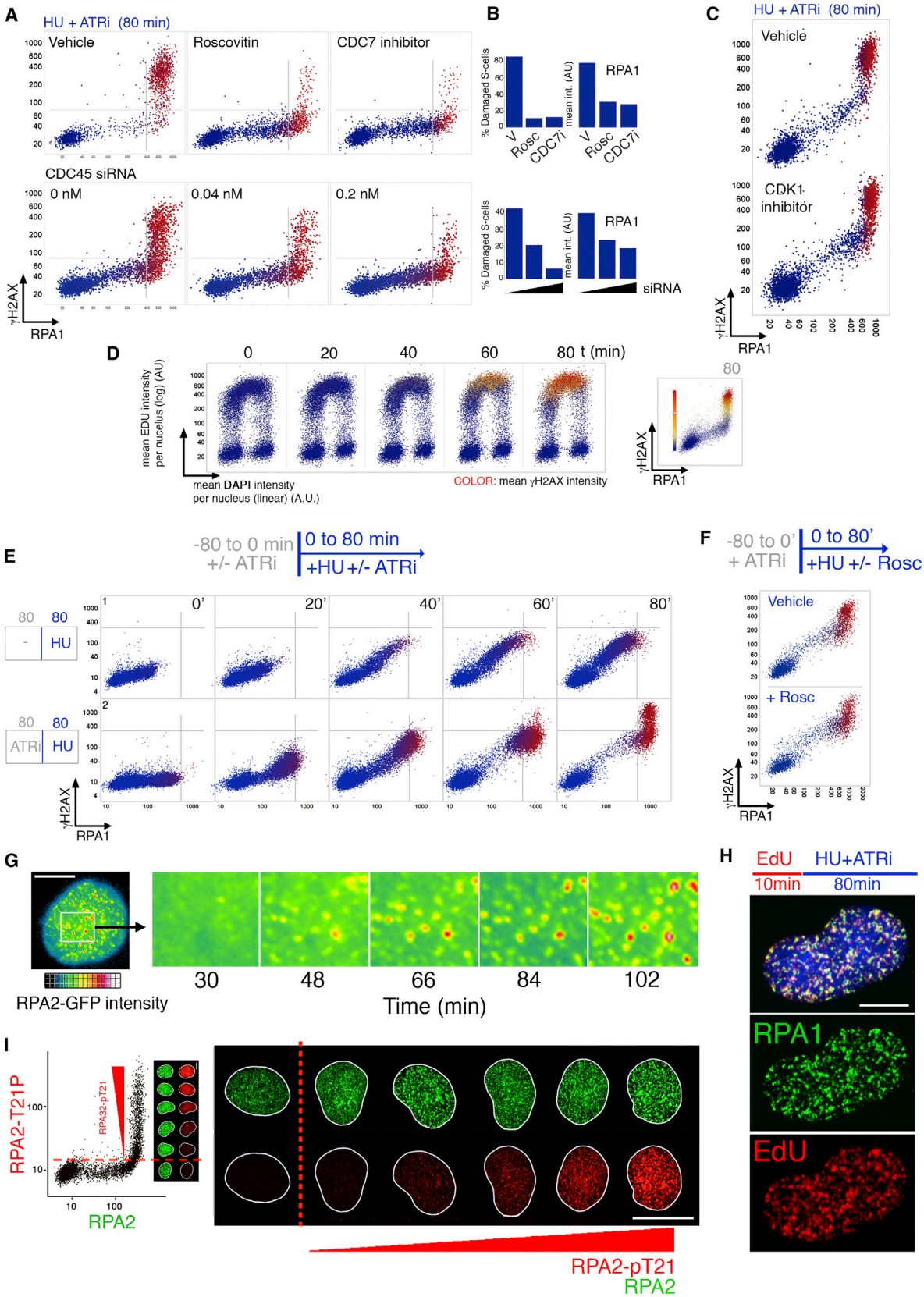

(legend on next page)

RPA buffering capacity (Figures S4D and S4E). Of note, the accelerated fork breakage occurred in cells with inhibited ATR, indicating that the ability of RPA to shield stalled forks is an autonomous mechanism that counteracts DNA breakage.

Stoichiometric Increase of the RPA Subunits Delays Fork Breakage

A reverse prediction was that a surplus of RPA should extend the dynamic range within which ATR-deficient cells escape fork breakage. To this end, we generated "SuperRPA" cell lines stably expressing 2- to 3-fold excess of all three RPA subunits, expressed from the same transcript in a stoichiometric fashion (Figures 4F, 4G, S4F, and S4G). Such degree of RPA overexpression did not alter DNA replication or ATR activation (Figures S4H and S4I). Strikingly, however, these cells dramatically extended the dynamic range of RPA loading on chromatin and became remarkably resilient to dNTP depletion and ATR inhibition at time points when cells with normal RPA levels underwent massive fork breakage (Figures 4H, 4I, S4J, and S4K). Furthermore, the acquired resilience of the SuperRPA cells was associated with reduced formation of unprotected ssDNA (Figure 4J). Because all of these experiments were performed in cells with inhibited ATR, we conclude that, as long as cells contain sufficient levels of RPA complex, it can be deployed to ssDNA and replication forks remain stable irrespective of ATR signaling. Of note, single overexpression of RPA1 subunits or other ssDNA-binding proteins such as hSSB1 or Rad51 did not prevent fork breakage after RPA depletion (L.I. Toledo and J. Lukas, unpublished data), indicating that the main cellular activity that can effectively shield replication intermediates against breakage is the fully assembled RPA complex, likely due to its exquisitely high affinity for ssDNA.

Exhaustion of the RPA Pool Generates Irreversible Damage to Replication Factories

Previous work indicated that forks exposed to replication stress eventually lose the ability to restart (Jossen and Bermejo, 2013). To test whether RPA exhaustion can explain this, we monitored the DSB dynamics in cells that were exposed to HU and ATRi for 2.5 hr (when the majority of S phase cells exhausted RPA and underwent DNA breakage) and were then released by removing both drugs (Figure 5A). Strikingly, 72 hr after the release, a fraction of cells still contained an unusually high number of RPA foci (100 foci per cell in average), indicating the presence of unrepaired forks (Figure 5B and Movie S4). After excluding contribution of undamaged cells, we could see that the fraction of cells with aberrant forks was very similar to that detected at the time of release from the HU/ATRi treatment (Figures S5A and S5B), suggesting that all such cells suffered a permanent proliferation blockade linked to irreparable fork breakage. Indeed, although cells with hallmarks of unrepaired forks could resume progression through S phase, likely due to replicons that were activated only after releasing from replication stress (Figure 5C and S5C), they all arrested at the G2-M boundary and eventually presented morphological features of senescence such as dramatic increase in size of cell nuclei (Figures 5C–5E). Thus, RPA exhaustion marks a "point of no return" for cell proliferation (Figure S5D).

To test whether such point of no return is reached exactly at the time of RPA exhaustion, we incubated cells with HU and ATRi for 40 min, when RPA loading approaches its threshold yet still without DNA breakage (Figure 2A), and then removed the drugs to stop any further RPA depletion. Under such conditions, RPA was rapidly unloaded from the chromatin (Figures 5F and 5G and Movie S5, top cell), whereas, when we extended the HU/ATRi treatment beyond the point of fork breakage (Figure 2B), an increasing fraction of cells failed to dissolve the RPA foci and arrested (Figure 5H and Movies S5, bottom cell, S6, and S7). Significantly, elevation of the RPA complex in the SuperRPA cell lines delayed this form of irreversible fork breakage (see Figures 4H–4J and S4K) and allowed recovery from the extended stress despite the fact that the overall ssDNA accumulation was 2- to 4-fold higher than in naive cells (Figures 5I and S5E). These results further support the model that RPA exhaustion, and not just an accumulation of supraphysiological levels of ssDNA, marks the point of no return. Furthermore, because ATR was inhibited in these experiments, the excess of RPA appears necessary and sufficient to shield supernumerary forks against breakage.

Figure 3. By Limiting Origin Firing, ATR Delays Exhaustion of RPA and Global Breakage of Active Forks

(A) U-2-OS cells treated with the general CDK inhibitor roscovitine (20 μM) or CDC7 inhibitor (20 μM) or transfected with CDC45 siRNA (indicated concentrations, 72 hr) were incubated with HU (2 mM) and ATRi (2 μM) for 80 min and were analyzed by QIBC.

(B) Quantification of QIBC plots from (A). (Right) Average values for RPA1 in S phase cells are shown.

(C) U-2-OS cells were treated and analyzed as in (A), combining HU and ATRi with a specific inhibitor of mitotic CDK1 (10 μM).

(D) U-2-OS cells were incubated with EdU (10 μM) for 30 min followed by HU (2 mM) and ATRi (2 μM) for the indicated times, pre-extracted, and immunostained as indicated. QIBC was performed, and mean DAPI, RPA1, γ-H2AX, and EdU (Click-it reaction) intensities per nucleus were obtained. DAPI/EdU replication profiles depicted in the scatter diagrams were color coded according to γ-H2AX intensity, which indicates the confinement of DSB to vigorously replicating cells.

(E) U-2-OS cells were incubated with HU (2 mM) and ATRi (2 μM) in the four described combinations and for the indicated times. QIBC for chromatin-loaded RPA1 and γ-H2AX was performed, and scatter diagrams for the two indicated combinations are shown (the rest are shown in Figure S3).

(F) U-2-OS cells were incubated with ATRi for 80 min, treated with HU with or without roscovitine for an additional 80 min, and analyzed by QIBC.

(G) U-2-OS cells stably expressing RPA2-EGFP were treated with HU (2 mM) and ATRi (2 μM), and fluorescence images of living cells were acquired every 2 min for up to 2 hr. Insets illustrate progressive loading of RPA into replication factories after ATR inhibition (see also Movie S1). Scale bar, 5 μm.

(H) U-2-OS cells were treated and processed as in (D), with the exception that the EdU was applied for 10 min. A representative picture is shown (80 min). Scale bar, 5 μm.

(I) U-2-OS cells were treated with HU (2 mM) and ATRi (2 μM) for 80 min, and QIBC was performed after RPA2 and RPA2-pT21 immunostainings. Representative images of nuclei with increasing levels of RPA2-pT21 were chosen, and their relative position in the QIBC diagram is indicated. Images show that all RPA foci are homogenously phosphorylated. Scale bar, 10 μm.

See also Figure S3.

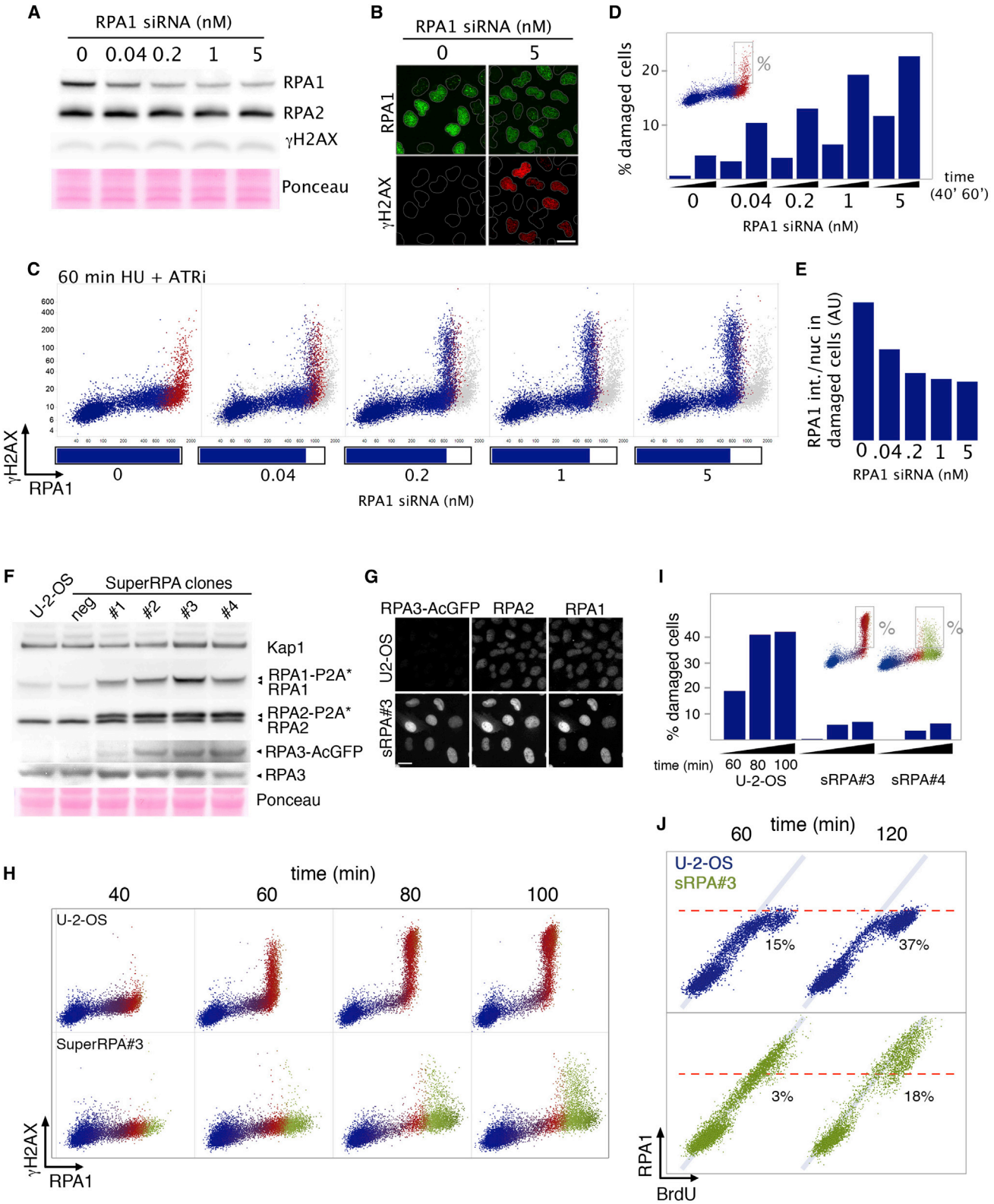

(legend on next page)

We reasoned that the accumulation of damaged cells in G2 is due to persistent checkpoint signaling from DNA lesions generated on stalled forks deprived from the RPA protection. Indicative of the presence of chromosome breaks, we observed cases of massive nuclear fragmentation in damaged cells that attempted to enter mitosis (Figure S5F). To validate that these lesions are bona fide DSBs, we pulse labeled active forks by EdU and then applied calyculin A, a phosphatase inhibitor that has been used as a tool to overcome cell-cycle checkpoints and induce premature chromosome condensation (El Achkar et al., 2005). Remarkably, virtually all metaphase spreads obtained after forcing the G2-arrested cells to mitosis were composed of shattered chromosomes with multiple breaks (Figures 5J, S5G, and S5H). Furthermore, the EdU signal was localized predominantly at sites with hallmarks of chromosome breaks such as terminal parts of shattered chromosomes or boundaries between fused chromosome fragments (Figures 5J, S5G, and S5H), supporting the conclusion that RPA exhaustion leads to the simultaneous breakage of active forks. Because of its fatal consequences, we henceforth refer to this event as "replication catastrophe" (RC).

RPA Exhaustion Is a Common Denominator of Replication Catastrophe, Regardless of the Source of Replication Stress or Unscheduled Origin Firing

A potential caveat of the previous results is that these were achieved under conditions in which replication stress imposed by HU was combined with unscheduled origin firing induced by ATRi. To validate that RPA shields stalled forks in a broader biological context, we revisited all major predictions by testing either drug alone and by using independent replication inhibitors and origin regulators. We first reasoned that, if the model is generally applicable, RPA should be rate limiting for fork breakage in cells that are treated with HU or ATRi alone because both treatments lead to steady generation of ssDNA (by helicase and polymerase uncoupling and unscheduled origin firing, respectively). Indeed, the increasing reduction of nuclear RPA levels leads to progressive fork breakage under these conditions (Figures 6A, 6B, and S6A). Thus, "single hits" of replication perturbation can eventually deplete the RPA pool, and combining them merely accelerates RPA depletion and the ensuing fork breakage.

The next prediction was that RPA should be rate limiting for active fork protection regardless of the sources of replication stress and/or unscheduled origin firing. This was also confirmed by experiments showing that independent inducers of fork stalling (aphidicolin, gemcitabine, citarabine, UV light) phenocopied HU by synergizing with ATRi in progressively depleting RPA up to the point of RC (Figures 6C and S6C). Likewise, the ATRi-induced RPA exhaustion was reproduced not only by inhibiting or depleting CHK1 (the downstream component of the ATR pathway), but also by inhibiting WEE1, another suppressor of unscheduled origin firing (Figures 6D and S6D). As predicted by the model, RC after CHK1 or WEE1 inhibition was mitigated by simultaneous suppression of origin firing (Figures 6E and S6E), and it showed strong correlation with the RPA levels when applied alone (Figure 6F and S6F), as well as when combined with distinct forms of replications stress (Figures 6G and S6G). Finally, the EdU-flanked chromosome breaks on calyculin A-induced metaphase spreads confirmed that the alternative sources of replication stress caused DSBs at active forks (Figures 6H and S6H). Thus, exhaustion of nuclear RPA represents a biological disaster for replicating genomes, regardless of the sources of replication stress or unscheduled origin firing.

DISCUSSION

Although ATR requires the RPA-coated ssDNA for its own activation, the endpoint of ATR signaling to protect forks against fatal breakage feeds back on the very same RPA by safeguarding its dynamic range and thus preventing exhaustion of this crucial molecular shield of replication intermediates (Figure 7A). The salient features of this mechanism are summarized in (Figures 7B–7D). When replication forks stall, the RPA-coated ssDNA generated ahead of the fork activates ATR. Although ATR per se remains confined to stalled forks, the pathway is propagated by CHK1, which diffuses away to suppress dormant origins. This limits the number of stalled forks to those that were active at the onset of the replication stress and ensures that RPA remains in excess over ssDNA (Figure 7B). If ATR signaling fails, dormant

Figure 4. RPA Levels Determine ssDNA Resilience to Breakage Independently of ATR

(A) U-2-OS cells were transfected with the indicated concentrations of siRNA against RPA1 for 40 hr, and WCE were immunoblotted with antibodies to the indicated RPA subunits and γ-H2AX.

(B) U-2-OS cells transfected as in (A) were treated with HU (2 mM) and ATRi (2 μM) for 40 and 60 min, pre-extracted, and immunostained with the indicated antibodies. Representative images (40 min time point) are shown. Scale bar, 10 μm.

(C) QIBC from immunostainings in (B). (Bottom bars) The degree of RPA1 knockdown at the point of fork breakage. Control U-2-OS diagrams obtained in cells with physiological levels of RPA (gray) serve as reference.

(D) Quantification of cells with DSBs in (C) at two different times (40 and 60 min) after HU and ATRi treatment.

(E) Average intensities of chromatin-bound RPA1 per nucleus from (D) (averaged from both time points).

(F) WCE from naive U-2-OS, a controlled U-2-OS cell line stably expressing free EGFP, and four different SuperRPA cell lines were immunoblotted with the indicated antibodies.

(G) Representative images of naive U-2-OS cells (top) and the SuperRPA cell line #3 (bottom) immunostained for total RPA1 and RPA2. RPA3 was visualized directly by GFP imaging (absent in naive U-2-OS cells). Scale bar, 10 μm.

(H) U-2-OS cell lines SuperRPA#3 and SuperRPA#4 (see Figure S5) were treated with HU (2 mM) and ATRi (2 μM) for the indicated times and were subjected to QIBC with the indicated antibodies. Green color in the scatter diagrams illustrates the excess of RPA1 loaded on the chromatin in RPA-overexpressing cells.

(I) Quantification of cells with DSB in (H) at the indicated time points.

(J) Control U-2-OS cell and SuperRPA#3 cell line were incubated with BrdU as in Figures 2E and 2F, treated with HU (2 mM) and ATRi (2 μM) for the indicated times, and subjected to QIBC. Percentages refer to cells with unprotected ssDNA.

See also Figure S4.

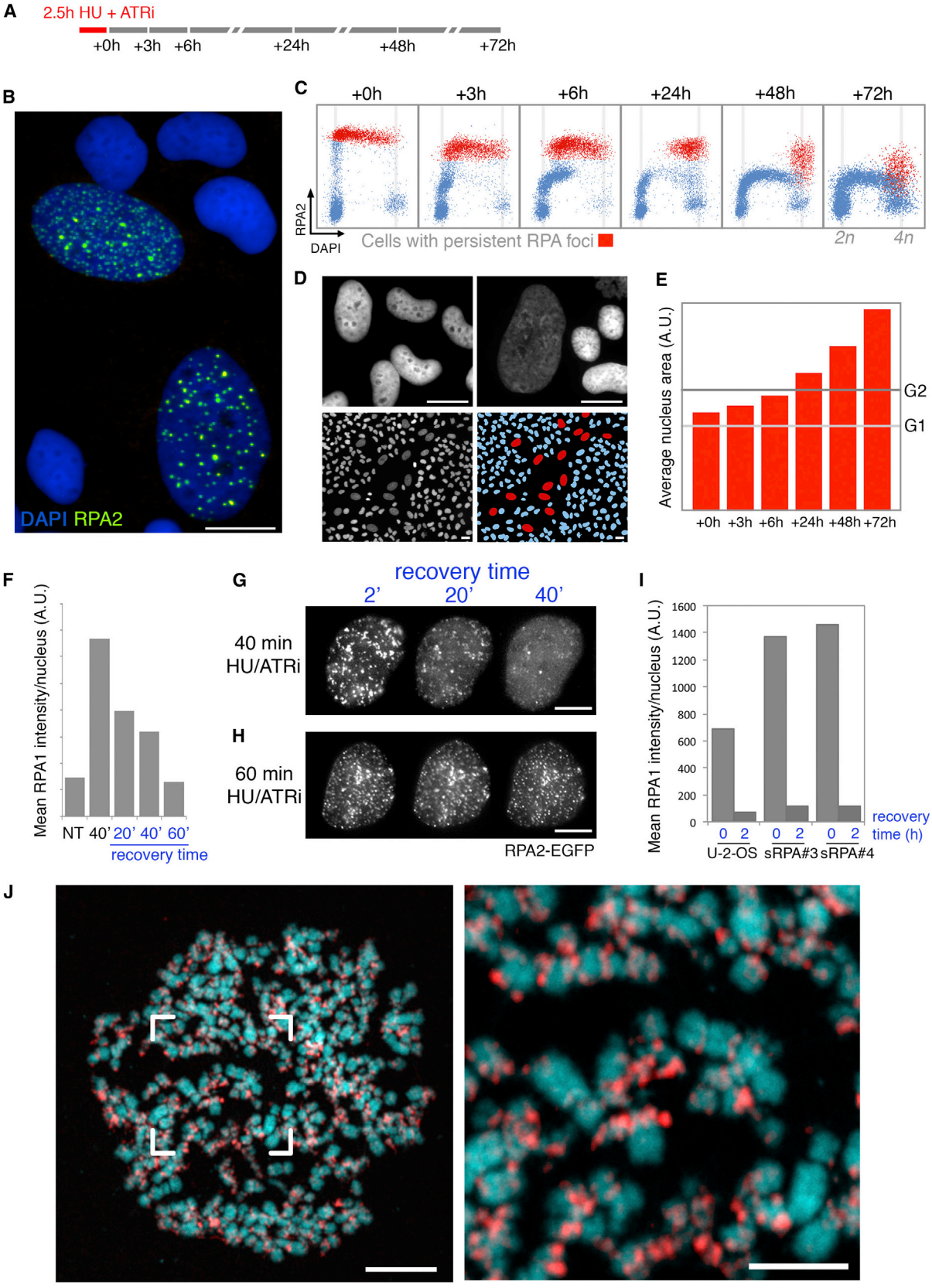

(legend on next page)

origins fire (Figure 7C), and the newly generated ssDNA progressively depletes nuclear RPA. When all RPA becomes sequestered, every active replicon generates unprotected ssDNA, which is rapidly converted to DSBs (Figure 7D).

We also show that RPA depletion in cells continuously exposed to replication stress triggers irreversible cell-cycle arrest. One scenario explaining this fatal consequence of replication stress is depicted in Figure 7E and reflects the model of eukaryotic replication whereby several loops of DNA, which may even originate from neighboring chromosomes, can be engaged in a single replicon (Cayrou et al., 2010). After sequestering all available RPA, every replicating loop would be prone to generate unprotected ssDNA, and the ensuing DNA breakage would dismantle the affected loci nucleus wide to an extent that would not be compatible with survival. In exceptional cases, RC might be confined to micronuclei, which result from chromosome misalignment and tend to undergo uncoordinated DNA replication (Crasta et al., 2012). Here, RPA exhaustion and the resulting chromosome disintegration might generate a precursor for chromothripsis, a cancer-related genomic abnormality characterized by erratic reassembly of previously "pulverized" DNA (Stephens et al., 2011).

Whereas we demonstrate that the excess of RPA determines fork resilience and effectively shields ssDNA intermediates under diverse stress conditions, our data do not exclude roles of other factors that, in a context-specific fashion, fine-tune fork protections against enzymatic processing that can ultimately lead to DSBs. One such example is the SMARCAL1-annealing nuclease, whose depletion delays DSB formation after ATR inhibition (Couch et al., 2013). It is possible that annealing helicases generate structures (such as the so-called reversed forks) that not only participate in RPA sequestration, but also generate substrates that can be processed by structure-specific nucleases, and thereby modulate the point at which RPA becomes exhausted.

An intriguing physiological ramification of our results includes common fragile sites (CFS), late-replicating genomic loci that undergo frequent breakage after various sources of replication stress, including oncogenic transformation (Debatisse et al., 2012). Although clearly triggered by replication stress, CFS breakage does not occur in S phase, but only in mitosis (Harrigan et al., 2011; Lukas et al., 2011). Our results elucidate this conundrum by showing the astonishing capacity of RPA to shield stalled forks way above the hypothetical situation when all currently known fragile sites encounter replication stress. However, RPA protection does not solve the problem of unfinished replication, explaining why CFS manifest as DSBs only in mitosis after structure-specific nucleases become hyperactivated and cleave underreplicated DNA (Naim et al., 2013; Ying et al., 2013). Interestingly, we note that RPA may not completely prevent intra-S-phase breakage of early replication fragile sites (ERFS) that, unlike CFS, replicate early and are largely confined to genomic loci that are highly transcriptionally active (Barlow et al., 2013). Under such circumstances, sporadic fork breakage can indeed happen even when RPA remains in excess due to the high stochastic probability of a collision between replication and transcription intermediates. This is analogous to a situation in cells deficient in single-strand DNA repair, whereby the nicks in DNA are converted to DSBs by the advancing replication forks, a situation that does not involve excessive ssDNA formation and thus cannot be prevented by RPA.

Interestingly, the concept of the RPA barrier against RC has intriguing evolutionary ramifications. The QIBC technique allowed us to estimate that the amount of ssDNA that a cell can tolerate, and therefore the excess of RPA required for shielding it, was ~8-fold higher than the amount required to support unperturbed DNA replication. This was unexpected because, from the thermodynamic perspective, proteins should not accumulate excessively unless this is physiologically pertinent. Strikingly, however, a similar surplus was reported for the nuclear pool of dormant origins licensed by the MCM helicase (Ge et al., 2007; Ibarra et al., 2008). Such excess of intrinsic replication potential turned out to be vital under replication stress, when the completion of genome replication becomes critically reliant on increased origin activity. Our data suggest that the surplus of RPA coevolved with dormant origins to "buffer" the excess of ssDNA during or after replication stress. Indeed, without

Figure 5. Fork Damage after RPA Exhaustion Is Irreversible and Drives Cells to a Permanent Cell-Cycle Arrest

(A) Schematic representation of the recovery assay. U-2-OS cells were treated with HU (2 mM) and ATRi (2 μM) for 2.5 hr and after replacing with fresh medium pre-extracted and fixed at the indicated time points.

(B) Representative image of U-2-OS cells immunostained for chromatin-bound RPA2 72 hr after release form HU/ATRi. Scale bar, 10 μm.

(C) QIBC scatter diagrams from cells in (B). Damaged S phase cells (red) progress through S phase after release from the stress and arrest in G2 (4n DNA content).

(D) (Top) Representative images of DAPI-stained undamaged and damaged cells, respectively (72 hr time point). Scale bar, 10 μm. (Bottom) Representative and color-coded fields containing DAPI-stained damaged (red) and undamaged (blue) cell nuclei (72 hr). Scale bar, 10 μm.

(E) Nuclear size of damaged cells was quantified by QIBC from data in (D) at the indicated times. Average area of G1 and G2 cells is annotated as a reference.

(F) U-2-OS cells were treated for 40 min with HU (2 mM) and ATRi (2 μM), released into drug-free media, and subjected to QIBC after the indicated times. Average values for chromatin-loaded RPA in S phase cells are depicted.

(G) RPA2-EGFP cells were treated for 40 min with HU (2 mM) and ATRi (2 μM), and time-lapse images were acquired after removing the drugs. Representative pictures are shown. Scale bar, 5 μm.

(H) Same as in (G) but with the extended treatment (60 min). Scale bar, 5 μm.

(I) SuperRPA cell lines (#3 and #4) and control U-2-OS cells were treated with HU (2 mM) and ATRi (2 μM) for 80 min, released into the drug-free medium for 2 hr, pre-extracted, and subjected to QIBC.

(J) A representative metaphase spread derived from a cell treated with HU and ATRi inhibitor for 80 min and allowed to recover for 40 hr. Active replicons were labeled with EdU for 10 min prior to the HU-induced replication stress. Premature chromosome condensation was induced by calyculin A (see Supplemental Information). (Right) Higher magnification of the indicated field. Scale bars: 10 μm (left), 5 μm (right).

See also Figure S5.

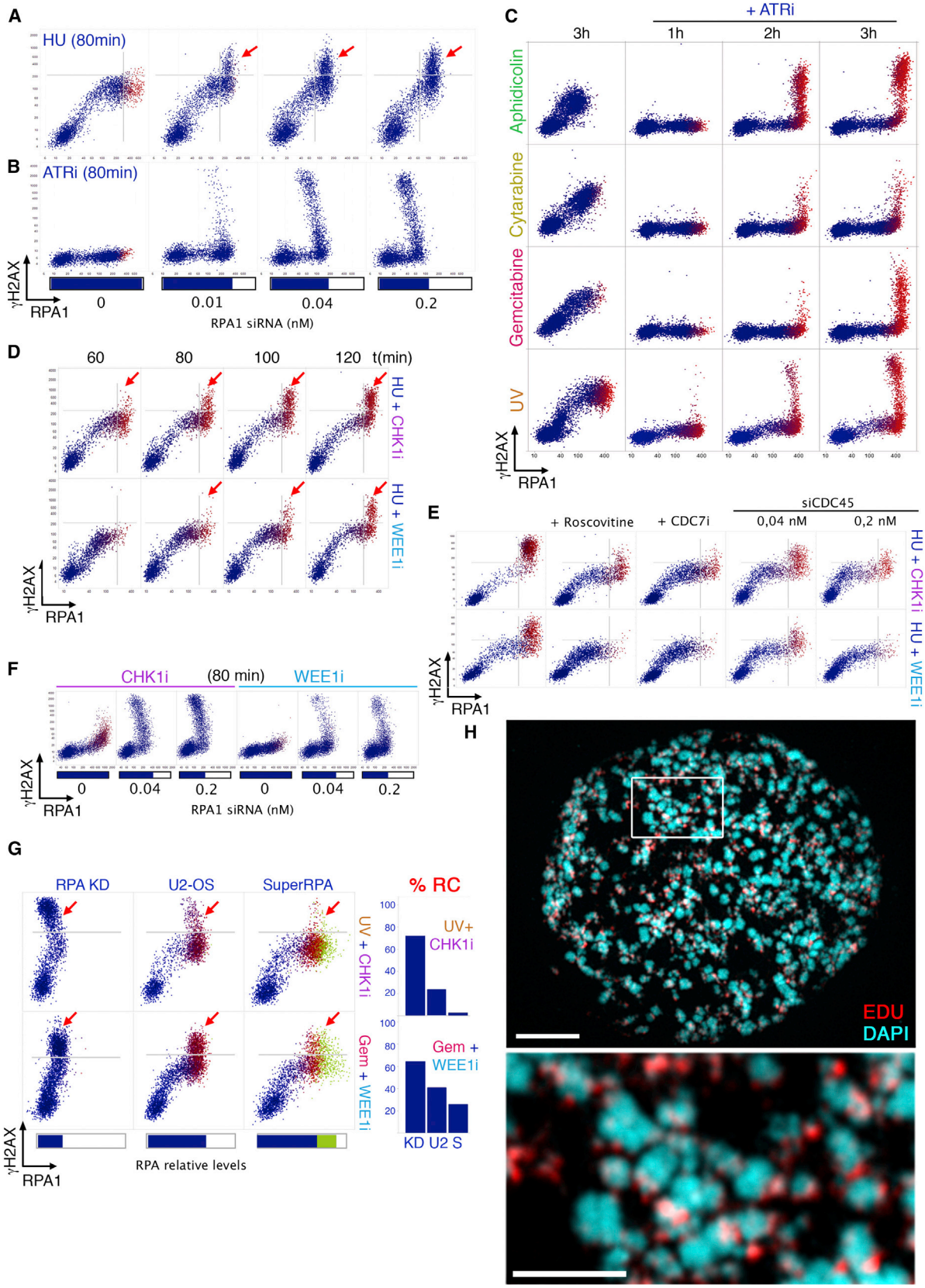

(legend on next page)

RPA protection, dormant origins could hardly be sustained during evolution because their activation would inevitably lead to replication catastrophe.

Finally, the global exhaustion of RPA described here can elucidate an increasing number of pathophysiological conditions that are linked with replication stress. First, cells derived from patients with the *Seckel* syndrome with hypomorphic ATR suffer massive replication stress associated with DNA breakage and premature senescence (Murga et al., 2009). We predicted that genomic instability in *Seckel* cells is fuelled by exhausting RPA due to uncontrolled replication, and we were indeed able to mimic this situation by using a specific ATR inhibitor. Second, oncogene transformation is accompanied by elevated replication stress (Halazonetis et al., 2008), and it has been shown that expression of oncogenes is synthetically lethal with ATR deficiency (Toledo et al., 2011). Based on our model, uncontrolled replication in oncogene-transformed cells is expected to reduce the intrinsic RPA buffer, explaining why ATR and/or CHK1 inhibitors show a remarkable selectivity in killing oncogene-transformed cells compared to normal cells (Toledo et al., 2011, Murga et al., 2011). Third, CHK1 inhibitors have shown a remarkable toxicity for tumor cells when combined with Gemcitabine in preclinical studies (Thompson and Eastman, 2013). This promising therapeutic approach essentially mimics the conditions used in this work to cause RPA exhaustion. Fourth, the reported correlation between high RPA level and increased therapeutic resistance in human cancer (Dahai et al., 2013; Givalos et al., 2007) indicates that enhanced expression and/or stability of RPA might be selected for during oncogenic transformation. This suggests that replication catastrophe might be a promising goal of current therapies aiming at efficient removal of cancer cells. Our data open up the possibility that modulating the RPA dynamic range might improve the efficacy of such treatments.

EXPERIMENTAL PROCEDURES

Plasmids and RNA Interference

cDNAs for human RPA subunits were provided by Marc S. Wold (University of Iowa, USA). P2A sequences were obtained as primers (Invitrogen). Cloning into pAc-GFP-C1 (Clontech) is described in the Supplemental Information. SiRNA duplexes were from Ambion (Silencer Select): ATR (s536), Cdc45 (s15829), Chk1 (s503), and RPA1 (s12127). Plasmid transfections were performed with Lipofectamine LTX and Plus Reagent (Invitrogen). siRNA transfections were performed with Lipofectamine RNAiMAX (Invitrogen). Unless specified, siRNAs were used at 25 nM. In siRNA titration assays, total siRNA concentration was kept constant with the addition of control siRNA.

Cell Culture

Human U-2-OS osteosarcoma, DLD1-ATR-*WildType*, and DLD1-ATR-*Seckel* colorectal cancer cells (Hurley et al., 2007) were grown in Dulbecco's modified Eagle's medium with 10% fetal bovine serum (GIBCO). For live imaging, cells were grown in CO2-independent medium (phenol red and riboflavin free, GIBCO). U-2-OS cell lines stably expressing ~2-fold excess of RPA2-EGFP were generated by standard procedures; RPA2-GFP avidly accumulated in replication factories regardless of replication stress. The AcGFP-RPA3-P2A-RPA1-P2A-RPA2 cell lines are characterized in Figures 4 and S4. Drugs and other cell culture supplements are described in the Supplemental Information.

Immunochemical and Biochemical Methods

Antibodies used for immunolabeling techniques are specified in the Supplemental Information. Whole-cell extracts (WCE) were obtained by lysis in RIPA buffer (50 mM Tris-HCl [pH 8.0], 150 mM NaCl, 1.0% Igepal CA-630, 0.1% SDS, 0.1% Na- deoxycholic acid, supplemented with protease and phosphatase inhibitors) containing $MgCl_2$ (2 mM) and Benzonase (Novagen) and analyzed by SDS-PAGE following standard procedures. For pre-extraction, cells were washed once with PBS and incubated with ice-cold PBS containing Triton X-100 (0.2%) for 1 min on ice prior to fixation. Immunostaining procedure is described in the Supplemental Information. EdU and TUNEL detection was performed by Click-it assay following manufacturer's instructions (Life Technologies).

Microscopy

Images used in QIBC were obtained with a motorized Olympus IX-81 wide-field microscope equipped with fast-switching filter wheels for excitation and emission of DAPI, FITC, Cy3, and Cy5 fluorescent dyes; an MT20 Illumination system; and a digital monochrome Hamamatsu C9100 CCD camera. Olympus UPLSAPO 10×/0.4 NA and 40×/0.9 NA objectives were used. Automated unbiased image acquisition was carried out by the propriety Scan acquisition software. For full description of QIBC see the Supplemental Information. Standard wide-field microscopy was performed on a Zeiss Axio Imager A2 equipped with EC Plan-Neofluar 10×/0.3, 20×/0.5, 40×/0.75 dry objectives, and an AxioCam MRm camera. Wide-field fluorescence time-lapse imaging was carried out on a Zeiss AxioObserver.Z1 microscope with a Zeiss Plan-APO 63×/1.4 oil-immersion objective and a Coolsnap HQ CCD camera (Roper Scientific) and on an ImageXpress Micro XL Wide-field Automated microscope with a Plan Fluor 40×/0.75 Nikon objective and a 4.66 megapixel scientific CMOS camera.

SUPPLEMENTAL INFORMATION

Supplemental Information includes Extended Experimental Procedures, six figures, and seven movies and can be found with this article online at http://dx.doi.org/10.1016/j.cell.2013.10.043.

Figure 6. RPA Exhaustion Is an Obligatory Step before Fork Breakage

(A) U-2-OS cells were transfected with the indicated concentrations of siRNA against RPA1 for 2 days, treated with HU as indicated, pre-extracted, immunostained with γH2AX and RPA1 antibodies, and analyzed by QIBC. Arrows mark cells with H2AX hyperphosphorylation corresponding to RC.

(B) U-2-OS cells were transfected as in (A), treated with ATRi as indicated, and analyzed as in (A).

(C) U-2-OS cells were incubated with the drugs (aphidicolin 20 μM, cytarabine 50 μM, gemcitabine 1 μM) or exposed to UV (20 J/m^2) as indicated, treated or not with ATRi, incubated for indicated times, and analyzed as in (A).

(D) U-2-OS cells were incubated with HU and the indicated inhibitors and analyzed as in (A).

(E) U-2-OS cells were transfected with the indicated siRNAs for 3 days, treated with the indicated inhibitors for 80 min, and analyzed as in (A).

(F) U-2-OS cells were transfected with the siRNA against RPA1 as in (A), treated with the indicated inhibitors, and after 80 min analyzed by QIBC.

(G) Naive U-2-OS cells, the same cells transfected with RPA1 siRNA for 2 days, or SuperRPA cells were treated with the indicated inhibitors and 120 min later analyzed by QIBC as in (A). The graphs on the right quantify the fraction of cells with signs of RC.

(H) A representative metaphase spread (see Figure 5J) derived from a U-2-OS cell treated with HU and WEE1 inhibitor for 80 min. Scale bars: 10 μm (top), 5 μm (bottom).

See also Figure S6.

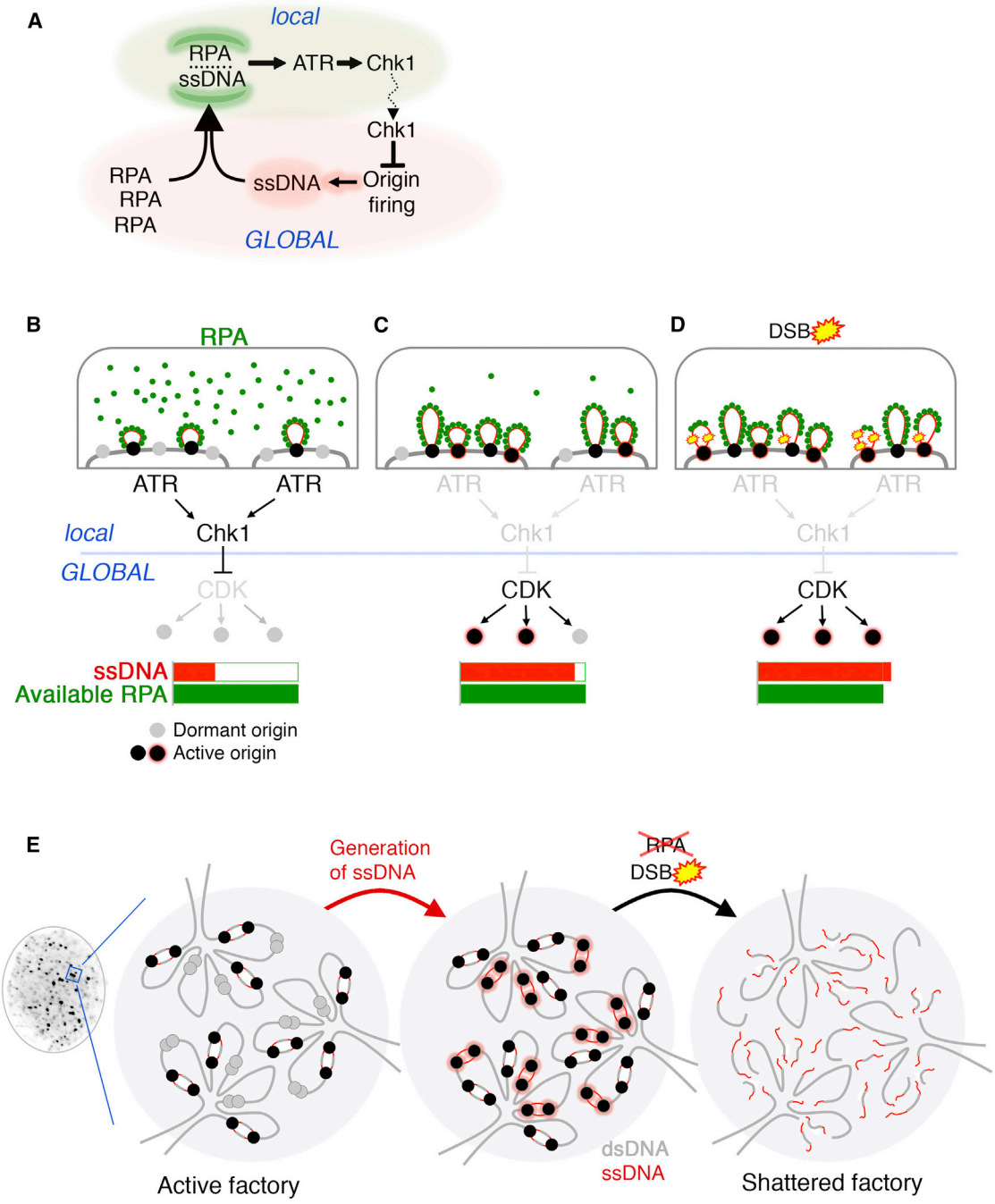

Figure 7. Model of Synchronized DNA Breakage at Replication Factories after RPA Exhaustion

(A) A feedback mechanism whereby ATR-CHK1 signaling ensures the maintenance of RPA surplus over ssDNA after replication stress.

(B–D) Inhibition of ATR or Chk1 triggers unscheduled firing of dormant origins, leading to a progressive RPA depletion, exposure of unprotected ssDNA, and massive DNA breakage.

(E) Graphical depiction for irreversible shattering of replication factories after ssDNA exceeds the RPA pool.

ACKNOWLEDGMENTS

We thank Drs. Oskar Fernandez-Capetillo (CNIO, Madrid) and Marc S. Wold (University of Iowa) for reagents and members of the Lukas lab for helpful comments on the manuscript. This work was supported by the Novo Nordisk Foundation, Danish Cancer Society, European Commission (Projects DDResponse and Biomedreg), and Danish National Research Foundation. L.I.T. and M.A. are recipients of long-term EMBO fellowships. We dedicate this paper to the

memory of Gabe Hayes, our handling editor at *Cell*, who tragically passed away. Gabe's unrestrained support of science and scientists, his insight, and his guidance of authors and reviewers will be sorely missed.

Received: May 16, 2013
Revised: August 19, 2013
Accepted: October 18, 2013
Published: November 21, 2013

REFERENCES

Barlow, J.H., Faryabi, R.B., Callén, E., Wong, N., Malhowski, A., Chen, H.T., Gutierrez-Cruz, G., Sun, H.W., McKinnon, P., Wright, G., et al. (2013). Identification of early replicating fragile sites that contribute to genome instability. Cell *152*, 620–632.

Branzei, D., and Foiani, M. (2009). The checkpoint response to replication stress. DNA Repair (Amst.) *8*, 1038–1046.

Brown, E.J., and Baltimore, D. (2000). ATR disruption leads to chromosomal fragmentation and early embryonic lethality. Genes Dev. *14*, 397–402.

Cayrou, C., Coulombe, P., and Méchali, M. (2010). Programming DNA replication origins and chromosome organization. Chromosome Res. *18*, 137–145.

Couch, F.B., Bansbach, C.E., Driscoll, R., Luzwick, J.W., Glick, G.G., Bétous, R., Carroll, C.M., Jung, S.Y., Qin, J., Cimprich, K.A., and Cortez, D. (2013). ATR phosphorylates SMARCAL1 to prevent replication fork collapse. Genes Dev. *27*, 1610–1623.

Crasta, K., Ganem, N.J., Dagher, R., Lantermann, A.B., Ivanova, E.V., Pan, Y., Nezi, L., Protopopov, A., Chowdhury, D., and Pellman, D. (2012). DNA breaks and chromosome pulverization from errors in mitosis. Nature *482*, 53–58.

Dahai, Y., Sanyuan, S., Hong, L., Di, Z., and Chong, Z. (2013). A relationship between replication protein A and occurrence and prognosis of esophageal carcinoma. Cell Biochem. Biophys. *67*, 175–180.

Debatisse, M., Le Tallec, B., Letessier, A., Dutrillaux, B., and Brison, O. (2012). Common fragile sites: mechanisms of instability revisited. Trends Genet. *28*, 22–32.

Eklund, H., Uhlin, U., Färnegårdh, M., Logan, D.T., and Nordlund, P. (2001). Structure and function of the radical enzyme ribonucleotide reductase. Prog. Biophys. Mol. Biol. *77*, 177–268.

El Achkar, E., Gerbault-Seureau, M., Muleris, M., Dutrillaux, B., and Debatisse, M. (2005). Premature condensation induces breaks at the interface of early and late replicating chromosome bands bearing common fragile sites. Proc. Natl. Acad. Sci. USA *102*, 18069–18074.

Fang, Y., Tsao, C.-C., Goodman, B.K., Furumai, R., Tirado, C.A., Abraham, R.T., and Wang, X.-F. (2004). ATR functions as a gene dosage-dependent tumor suppressor on a mismatch repair-deficient background. EMBO J. *23*, 3164–3174.

Fanning, E., Klimovich, V., and Nager, A.R. (2006). A dynamic model for replication protein A (RPA) function in DNA processing pathways. Nucleic Acids Res. *34*, 4126–4137.

Fekairi, S., Scaglione, S., Chahwan, C., Taylor, E.R., Tissier, A., Coulon, S., Dong, M.-Q., Ruse, C., Yates, J.R., 3rd, Russell, P., et al. (2009). Human SLX4 is a Holliday junction resolvase subunit that binds multiple DNA repair/recombination endonucleases. Cell *138*, 78–89.

Forment, J.V., Blasius, M., Guerini, I., and Jackson, S.P. (2011). Structure-specific DNA endonuclease Mus81/Eme1 generates DNA damage caused by Chk1 inactivation. PLoS ONE *6*, e23517.

Friedel, A.M., Pike, B.L., and Gasser, S.M. (2009). ATR/Mec1: coordinating fork stability and repair. Curr. Opin. Cell Biol. *21*, 237–244.

Ge, X.Q., Jackson, D.A., and Blow, J.J. (2007). Dormant origins licensed by excess Mcm2-7 are required for human cells to survive replicative stress. Genes Dev. *21*, 3331–3341.

Gillespie, P.J., and Blow, J.J. (2010). Clusters, factories and domains: The complex structure of S-phase comes into focus. Cell Cycle *9*, 3218–3226.

Givalos, N., Gakiopoulou, H., Skliri, M., Bousboukea, K., Konstantinidou, A.E., Korkolopoulou, P., Lelouda, M., Kouraklis, G., Patsouris, E., and Karatzas, G. (2007). Replication protein A is an independent prognostic indicator with potential therapeutic implications in colon cancer. Mod. Pathol. *20*, 159–166.

Halazonetis, T.D., Gorgoulis, V.G., and Bartek, J. (2008). An oncogene-induced DNA damage model for cancer development. Science *319*, 1352–1355.

Hanada, K., Budzowska, M., Davies, S.L., van Drunen, E., Onizawa, H., Beverloo, H.B., Maas, A., Essers, J., Hickson, I.D., and Kanaar, R. (2007). The structure-specific endonuclease Mus81 contributes to replication restart by generating double-strand DNA breaks. Nat. Struct. Mol. Biol. *14*, 1096–1104.

Harrigan, J.A., Belotserkovskaya, R., Coates, J., Dimitrova, D.S., Polo, S.E., Bradshaw, C.R., Fraser, P., and Jackson, S.P. (2011). Replication stress induces 53BP1-containing OPT domains in G1 cells. J. Cell Biol. *193*, 97–108.

Hurley, P.J., Wilsker, D., and Bunz, F. (2007). Human cancer cells require ATR for cell cycle progression following exposure to ionizing radiation. Oncogene *26*, 2535–2542.

Ibarra, A., Schwob, E., and Méndez, J. (2008). Excess MCM proteins protect human cells from replicative stress by licensing backup origins of replication. Proc. Natl. Acad. Sci. USA *105*, 8956–8961.

Jossen, R., and Bermejo, R. (2013). The DNA damage checkpoint response to replication stress: A Game of Forks. Front. Genet. *4*, 26.

Lambert, S., and Carr, A.M. (2005). Checkpoint responses to replication fork barriers. Biochimie *87*, 591–602.

Lukas, C., Savic, V., Bekker-Jensen, S., Doil, C., Neumann, B., Pedersen, R.S., Grøfte, M., Chan, K.L., Hickson, I.D., Bartek, J., and Lukas, J. (2011). 53BP1 nuclear bodies form around DNA lesions generated by mitotic transmission of chromosomes under replication stress. Nat. Cell Biol. *13*, 243–253.

Matos, J., Blanco, M.G., and West, S.C. (2013). Cell-cycle kinases coordinate the resolution of recombination intermediates with chromosome segregation. Cell reports *4*, 76–86.

Murga, M., Bunting, S., Montaña, M.F., Soria, R., Mulero, F., Cañamero, M., Lee, Y., McKinnon, P.J., Nussenzweig, A., and Fernandez-Capetillo, O. (2009). A mouse model of ATR-Seckel shows embryonic replicative stress and accelerated aging. Nat. Genet. *41*, 891–898.

Murga, M., Campaner, S., Lopez-Contreras, A.J., Toledo, L.I., Soria, R., Montaña, M.F., D'Artista, L., Schleker, T., Guerra, C., Garcia, E., et al. (2011). Exploiting oncogene-induced replicative stress for the selective killing of Myc-driven tumors. Nat. Struct. Mol. Biol. *18*, 1331–1335.

Naim, V., Wilhelm, T., Debatisse, M., and Rosselli, F. (2013). ERCC1 and MUS81-EME1 promote sister chromatid separation by processing late replication intermediates at common fragile sites during mitosis. Nat. Cell Biol. *15*, 1008–1015.

Petermann, E., Orta, M.L., Issaeva, N., Schultz, N., and Helleday, T. (2010). Hydroxyurea-stalled replication forks become progressively inactivated and require two different RAD51-mediated pathways for restart and repair. Mol. Cell *37*, 492–502.

Sørensen, C.S., and Syljuåsen, R.G. (2012). Safeguarding genome integrity: the checkpoint kinases ATR, CHK1 and WEE1 restrain CDK activity during normal DNA replication. Nucleic Acids Res. *40*, 477–486.

Stephens, P.J., Greenman, C.D., Fu, B., Yang, F., Bignell, G.R., Mudie, L.J., Pleasance, E.D., Lau, K.W., Beare, D., Stebbings, L.A., et al. (2011). Massive genomic rearrangement acquired in a single catastrophic event during cancer development. Cell *144*, 27–40.

Tercero, J.A., Longhese, M.P., and Diffley, J.F.X. (2003). A central role for DNA replication forks in checkpoint activation and response. Mol. Cell *11*, 1323–1336.

Thompson, R., and Eastman, A. (2013). The cancer therapeutic potential of Chk1 inhibitors: how mechanistic studies impact on clinical trial design. Br. J. Clin. Pharmacol. *76*, 358–369.

Toledo, L.I., Murga, M., Zur, R., Soria, R., Rodriguez, A., Martinez, S., Oyarzabal, J., Pastor, J., Bischoff, J.R., and Fernandez-Capetillo, O. (2011). A cell-based screen identifies ATR inhibitors with synthetic lethal properties for cancer-associated mutations. Nat. Struct. Mol. Biol. *18*, 721–727.

Trenz, K., Smith, E., Smith, S., and Costanzo, V. (2006). ATM and ATR promote Mre11 dependent restart of collapsed replication forks and prevent accumulation of DNA breaks. EMBO J. *25*, 1764–1774.

Ying, S., Minocherhomji, S., Chan, K.L., Palmai-Pallag, T., Chu, W.K., Wass, T., Mankouri, H.W., Liu, Y., and Hickson, I.D. (2013). MUS81 promotes common fragile site expression. Nat. Cell Biol. *15*, 1001–1007.